RSC Advances

PAPER

View Article Online
View Journal | View Issue

Cite this: *RSC Adv.*, 2026, **16**, 916

Prediction of miscibility in chlorinated polyethylene/poly(vinyl chloride) blends *via* atomistic molecular dynamics simulations

Zhihao Ma,[a] Xue Li,*[b] Huaguo Xu,[a] Jianxiang Shen *[ac] and Jun Liu[c]

The miscibility of chlorinated polyethylene (CPE)/polyvinyl chloride (PVC) blends is intricately influenced by both chemical structures and environmental conditions. This study employs all-atom molecular dynamics simulations to systematically investigate the effects of CPE chlorine content and molecular architecture, blend composition, and temperature on CPE/PVC miscibility behavior. Analysis of solubility parameters (δ) suggests that the compatibility of CPE/PVC blends improves with increasing chlorine content within the examined range. Random-chlorinated polyethylene (r-CPE) demonstrates superior miscibility with PVC compared to block-chlorinated polyethylene (b-CPE), attributed to enhanced electrostatic contributions arising from intensified polar Cl–Cl interactions. CPE/PVC blends containing approximately 20–80 wt% CPE are found to be thermodynamically immiscible at 300 K. Furthermore, a quantitative relationship between the Flory–Huggins interaction parameter (χ_{12}) and temperature (T) is established, revealing an increase in χ_{12} with T, indicative of reduced miscibility at higher temperatures. The phase diagram exhibits a low critical solution temperature (LCST) behavior, consistent with the χ_{12}–T relationships. Notably, r-CPE/PVC binary systems exhibit a higher LCST critical temperature (T_{cr}) than b-CPE/PVC systems. In general, this simulation study provides better understandings of CPE/PVC miscibility and offers valuable guidance for the design and optimization of CPE/PVC composite materials.

Received 10th December 2025
Accepted 19th December 2025

DOI: 10.1039/d5ra09560c

rsc.li/rsc-advances

1 Introduction

Polyvinyl chloride (PVC) is a widely used synthetic polymer renowned for its versatility, durability, and cost-effectiveness.[1–3] However, its performance is somewhat hindered by brittleness at low temperatures, limiting its applications in cold climates.[4–7] To address this issue, various modification strategies have been explored,[8–10] including the incorporation of rubber modifiers like acrylic rubber (ACR),[11] acrylonitrile–butadiene–styrene (ABS),[12,13] and nitrile butadiene rubber (NBR),[14,15] as well as other modifiers such as polymethyl methacrylate (PMMA),[16,17] methyl methacrylate–butadiene–styrene (MBS),[18,19] dioctyl phthalate (DOP),[20] and chlorinated polyethylene (CPE).[21] For example, our recent work combined all-atom molecular dynamics (MD) simulation and experimental tools to investigate the mechanical properties of PVC/$CaCO_3$ nanocomposites, and the results indicated that 12 wt% $CaCO_3$ modified with oleate anion and dodecylbenzenesulfonate can impart high toughness to PVC.

Chlorinated polyethylene (CPE), derived from high-density polyethylene (HDPE) through chlorine substitution, offers a promising approach to modifying PVC.[22,23] Its structural similarity to PVC, with the introduction of polar groups, enhances compatibility and improves toughness.[24] CPE/PVC blends have been shown to form partially thermodynamically compatible systems, leading to improved mechanical properties.[25] However, CPE and PVC are probably segmental immiscible, while CPE exhibits good compatibility with polyethylene (PE). To improve the CPE/PVC blend miscibility, nanoparticles are usually added into CPE/PVC blends functionalizing as interfacial compatibilizer. For instance, You *et al.* investigated the brittle–ductile transition in CPE/PVC blends, finding that CPE and nano-$CaCO_3$ can enhance both mechanical properties and toughness.[21] Their results indicated that CPE plays a more significant role than PVC in determining the brittle–ductile transition temperature, while nano-$CaCO_3$ has a minimal impact. Recent work by Zhang *et al.* also demonstrated that increasing CPE could significantly improve the impact resistance and thermal stability of the PVC composites.[26]

To optimize the performance of CPE/PVC blends, a deep understanding of their thermodynamic compatibility is essential. However, although many experimental studies have explored CPE/PVC blend compatibility, precise control of experimental parameters can be challenging due to their interconnected nature. Computational simulations offer

[a]*Department of Polymer Science and Technology, Jiaxing University, Jiaxing 314001, China. E-mail: shenjx@zjxu.edu.cn*

[b]*School of Advanced Materials Engineering, Jiaxing Nanhu University, Jiaxing 314001, China. E-mail: lixue@jxnhu.edu.cn*

[c]*State Key Laboratory of Organic–Inorganic Composites, Beijing University of Chemical Technology, Beijing 100029, China*

a powerful tool to predict polymer blend miscibility, particularly for systems that are difficult to study experimentally.[27–29] For instance, using molecular dynamics simulation, the miscibility in polylactide/polyvinilphenol blends was analyzed.[30] Jawalkar *et al.* employed atomistic MD simulations to investigate the compatibility of poly(vinyl alcohol) and chitosan blends.[31] Their simulation results showed good agreement with experimental data, demonstrating the reliability of this approach. Besides, Patnaik *et al.* studied the miscibility behavior of PMMA/4-*n*-pentyl-4′-cyanobiphenyl binary mixtures, a blend of polymeric and low molecular weight molecules, using a combination of modified Flory–Huggins theory and molecular simulation techniques.[32] Costa *et al.* investigated the solubility of hydrophobic or hydrophilic polymers in aliphatic cyclohexane, and compared Flory–Huggins interaction parameters (χ_{12}) using three different molecular dynamics simulation approaches.[33] Their results indicated that χ_{12} obtained from the enthalpy of solvation and Gibbs free energy of solvation were more accurate than that calculated from Hildebrand solubility parameters of the pure components.

While significant attention has been directed towards the molecular simulation of polymer blend miscibility, the CPE/PVC blend system remains relatively unexplored. In this study, we employ all-atom molecular dynamics (MD) simulations to investigate the miscibility behavior of CPE/PVC blends, by varying CPE chlorine content and molecular architecture, blend ratio, and temperature. We systematically examine the cohesive energy density (C.E.D.), solubility parameters (δ), Flory–Huggins interaction parameter (χ_{12}), Gibbs free energy (ΔG), and phase diagrams to evaluate the blend compatibility. Notably, some of our simulation results align well with experimental observations. Our findings could provide some guidance on the design and production of CPE/PVC composites in industrial applications.

2 Simulation models and method

2.1 All-atom models

In this work, atomistic models of CPE/PVC blends were constructed using Avogadro software.[34] The CPE chains were generated by replacing some hydrogen atoms with chlorine atoms. Each chain consisted of 20 repeat units, sufficient to capture structural and dynamic characteristics of longer chains.[33] The total number of atoms in the system was more than 4000. Each chain consisted of 20 repeat units, which is sufficient to capture structural and dynamic characteristics of longer chains, while intentionally excluding the effects of chain entanglement.[35] Although certain quantitative values (*e.g.*, C.E.D. and δ) may display some chain-length dependence, we believe the main conclusions of our study in the qualitive and even certain quantitative aspects should remain robust. The chlorine content (Cl wt%) of CPE is defined by

$$\mathrm{Cl}\% = \frac{\Delta w \frac{34.5}{36.5}}{w + \Delta w \frac{34.5}{36.5}} \times 100\%, \quad (1)$$

where w is the mass fraction of the molecular chain and Δw is the difference in mass. PVC contains 56.7 wt% Cl. In this work, the Cl wt% of CPE investigated ranges from 26.9% to 42.4%, falling within the established immiscibility window with PVC (the lower bound of miscibility ≈ 44 wt% (ref. 36)). In fact, CPEs with 25–40 wt% Cl are considered to be optimal impact modifiers due to their practical compatibility,[25] underscoring our selection of these CPE models to specifically address the enhancement of PVC toughness. Detailed information about the modeled CPE is provided in Table 1.

To investigate the effects of CPE chain architecture on CPE/PVC miscibility, two CPE types were established in this study, *i.e.*, random CPE (r-CPE) and block CPE (b-CPE), distinguished by their Cl atom distribution along the molecular chain. Fig. 1 illustrates examples of r-CPE and b-CPE chains.

For each modeled system, the COMPASS (Condensed-Phase Optimized Molecular Potentials for Atomistic Simulation Studies) force field[37] was employed in the molecular dynamics (MD) simulations. This force field is well-suited for characterizing polymer blending systems and accurately predicting the miscibility properties of polymeric mixtures. The COMPASS force field ensures a high degree of accuracy by comprehensively accounting for the total potential energy, including bond interactions, cross-coupling terms, and non-bond energies. Within the LAMMPS (Large-scale Atomic/Molecular Massively Parallel Simulator) software,[38] the COMPASS force field is implemented *via* the CLASS2 package, which accounts for bonded interactions (bonds, angles, dihedrals, improper) and non-bonded interactions.[39] Specifically, the non-bonded interactions are depicted as the summation of van der Waals forces and electrostatic interactions, as given by

$$E_{\text{non-bond}} = E_{\text{van der Waals}} + E_{\text{electrostatic}} \quad (2)$$

$$E_{\text{van der Waals}} = \sum_{ij} \varepsilon_{ij} \left[2\left(\frac{r_{ij}^{0}}{r_{ij}}\right)^{9} - 3\left(\frac{r_{ij}^{0}}{r_{ij}}\right)^{6} \right] \quad (3)$$

$$E_{\text{electrostatic}} = \sum_{ij} \frac{q_i q_j}{r_{ij}}, \quad (4)$$

where both are cut off at the distance of 9.5 Å. Standard Ewald summations are employed to compute the electrostatic interactions. The COMPASS force field, as realized in the CLASS2 package, has been demonstrated to be both effective and

Table 1 Details of CPE models in the study

No. of Cl atoms per chain	Degree of polymerization	Cl wt% of CPE
6	20	26.9%
7		30.0%
8		32.9%
9		35.6%
10		38.0%
11		40.3%
12		42.4%

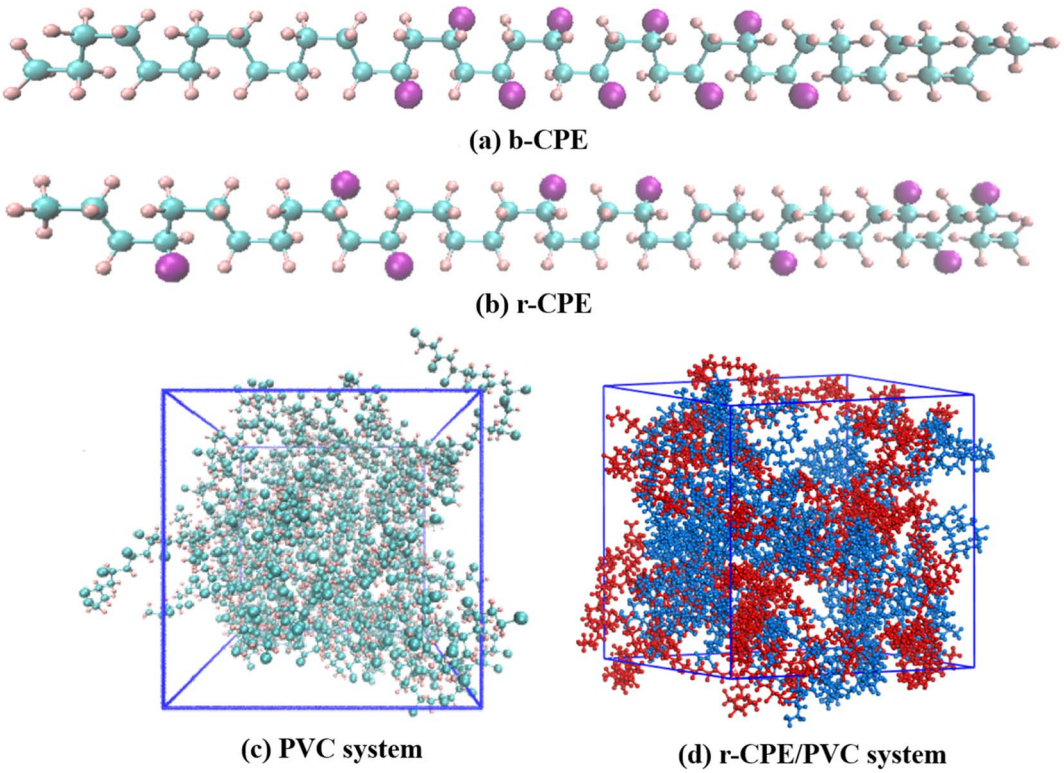

Fig. 1 Representative molecular models of (a) block CPE (b-CPE), (b) random CPE (r-CPE), both with 35.6 wt% Cl, (c) pure PVC system, and (d) r-CPE/PVC blend system. Purple, cyan, and pink atoms represent chlorine (Cl), carbon (C), and hydrogen (H), respectively. In panel (d), PVC chains are colored blue and r-CPE chains are red for visual distinction.

accurate in modeling polymeric materials, which has also been shown in our previous atomistic MD studies on the SWNT/TPU composite model[40] and the C_{60}/TPU composite model.[41] The CPE/PVC composite systems investigated in our simulations comprised materials with varying CPE (r-CPE with 35.6 Cl wt%) to PVC ratios, as detailed in Table 2.

2.2 Molecular dynamics simulation

All molecular dynamics (MD) simulations were performed using LAMMPS.[38] The system was initialized with non-overlapping polymer chain configurations in a large simulation box. Following energy minimization *via* the steepest descent algorithm, the system was further equilibrated under isothermal–isobaric (NPT) ensemble conditions at a pressure of 0.1 MPa and a temperature of 300 K for a duration of 1 ns. The Nose–Hoover thermostat and barostat[42,43] were employed to control temperature and pressure, respectively, while Newtonian equations of motion were integrated using the velocity-Verlet algorithm with a time step of 1 fs. Three-dimensional periodic boundary conditions were applied throughout to reduce the finite-size effects. Fig. 1c and d show some of the simulation systems under equilibrium. After sufficient equilibration, configurations were recorded every 2 ps over an additional 500 ps NPT simulation. To investigate the temperature-dependent miscibility behavior of the CPE/PVC blends (Section 3.3), MD simulations were also conducted across a broader range (250 K, 300 K, 350 K, 400 K, and 450 K), spanning both the glassy and rubbery regimes of PVC ($T_g \approx 370$ K). Fig. 2 depicts the evolution of PVC density and system energies as a function of simulation time. It is evident from the figure that the system rapidly reaches equilibrium within the initial 50 ps. In addition, to assess the conformational equilibration at the chain level, the time evolution of the radius of gyration (R_g) was also monitored (Fig. 3). The R_g time series likewise converges quickly to a stable value, indicating that the polymer chains have achieved conformational equilibrium. Together, the convergence of bulk thermodynamic properties and chain conformations corroborates that the systems reach equilibrium on the stated timescale. It should be noted that, unless otherwise specified, all numerical values presented in the tables and principal comparative analysis correspond to the reference temperature of 300 K.

Table 2 CPE/PVC composites examined in the study

System no.	No. of PVC chains in composite	PVC wt%	CPE wt%
1	20	100%	0%
2	17	87.8%	12.2%
3	14	74.1%	25.9%
4	10	58.9%	41.1%
5	7	41.8%	58.2%
6	5	30.4%	69.6%
7	4	22.3%	77.7%
8	2	13.7%	86.3%
9	0	0%	100%

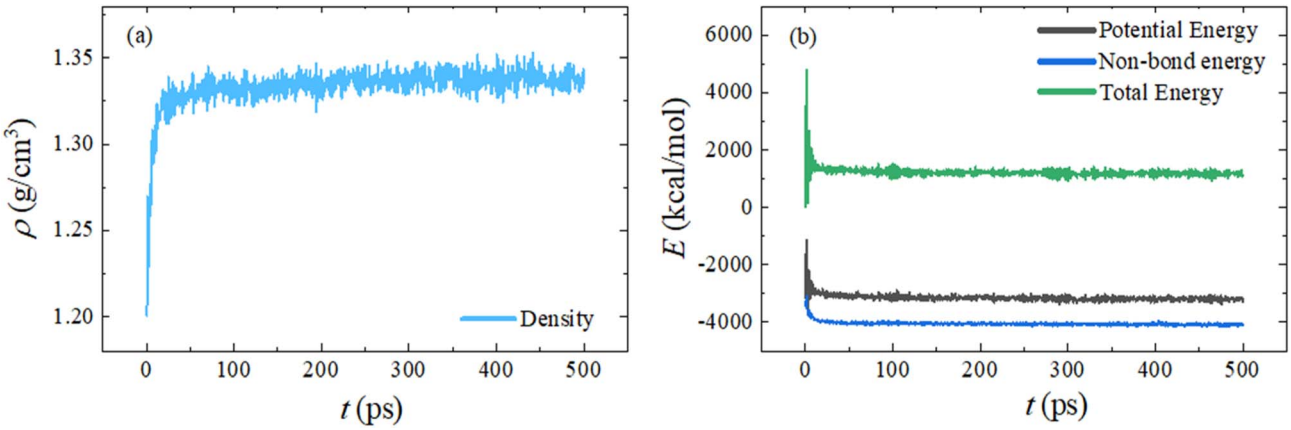

Fig. 2 Variations in (a) PVC density and (b) system energies as a function of time over the initial 500 ps.

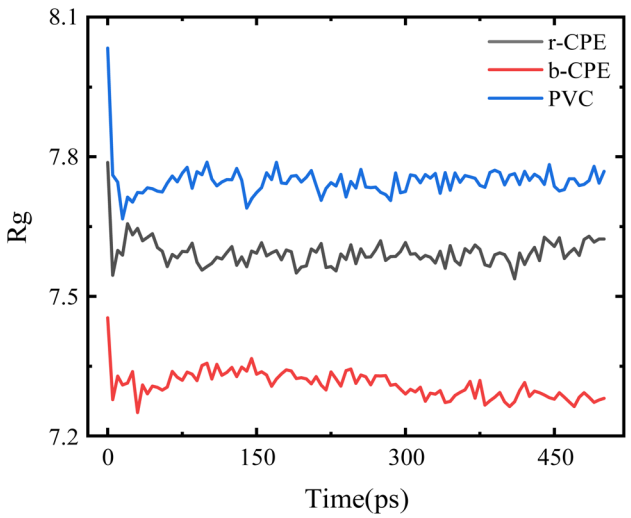

Fig. 3 Time evolution of the radius of gyration (R_g) of the PVC, r-CPE, b-CPE chains.

We further validated our simulation results by comparing key parameters, including polymer density (ρ) and solubility parameter (δ), with experimental values, as summarized in Table 3. Experimental reference data for density and solubility parameters are reported at 298 K, whereas all simulation results in this work were obtained at 300 K. As shown, the values of ρ and δ obtained from our MD simulations fall within the ranges reported experimentally. The close agreement between the simulation results and the experimental measurements highlights the reliability and accuracy of our computational approach.

3 Results and discussion

3.1 Effects of CPE chlorine content

3.1.1 Hildebrand solubility parameter. To quantify the impact of CPE on CPE/PVC blend compatibility, we first calculate the Hildebrand solubility parameter for CPE. The solubility parameter reflects the cohesive energy density and thus can be a good indicator to characterize the intermolecular interactions within a material. The solubility parameter, δ, is defined as the square root of cohesive energy density,[46] which is written as

$$\delta = \sqrt{\frac{E_{coh}}{V}} = \sqrt{\frac{\Delta H_v - RT}{V}}, \quad (5)$$

where E_{coh} represents the change in internal energy upon vaporization, *i.e.*, the energy required to separate all molecules; R is the molar gas constant (8.314 J mol^{-1} K^{-1}), and T is the simulation temperature (400 K in this study). In this work, E_{coh} can be determined by averaging all intermolecular non-bonded energy over simulation time,[40]

$$\delta = \sqrt{-\frac{\left\langle \sum_{i=1}^{n-1} \sum_{j=i+1}^{n} E_{i,j} \right\rangle}{\langle V \rangle}}, \quad (6)$$

where $E_{i,j}$ is the total non-bonded energy, and $\langle \ldots \rangle$ denotes the time average over MD simulation time after sufficient equilibrium.

Table 3 Comparison of our simulation results with experimental values

	Density (g cm^{-3})		Solubility parameter (MPa$^{0.5}$)	
Polymers	MD simulations[a]	Experiments[b]	MD simulations	Experiments
b-CPE	1.301 ± 0.004	1.15–1.25	—	—
r-CPE	1.322 ± 0.004	1.15–1.25	—	—
PVC	1.338 ± 0.005	1.34 (ref. 44), 1.35–1.45	21.20 ± 0.11	23.10 (ref. 45), 21.92 (ref. 36)

[a] MD simulation data were all obtained at a temperature of 300 K. [b] Experimental data were obtained at room temperature.

Table 4 summarizes the solubility parameters (δ) of CPE as a function of chlorine content (Cl wt%). To facilitate visual interpretation, Fig. 4 illustrates the corresponding trends in δ for both b-CPE and r-CPE. A consistent increase in δ with rising Cl% is observed for both b-CPE and r-CPE, consistent with findings from prior studies. Notably, r-CPE exhibits a higher δ than b-CPE at equivalent Cl%, suggesting stronger intermolecular interactions in the randomly chlorinated system. At low Cl wt% (*e.g.*, 26.88 wt%), the difference in δ between r-CPE and b-CPE is minimal; however, this disparity grows markedly with increasing Cl wt%. Such a discrepancy is likely attributed to the microphase separation of polar –CH_2–CHCl– segments from nonpolar –CH_2–CH_2– units within the b-CPE polymer, which diminishes the interchain dipole–dipole interactions mediated by Cl atoms. This hypothesis is corroborated by the observed large divergence in electrostatic solubility parameters (Fig. 5), as discussed subsequently.

We further compute the absolute solubility parameter differences between CPE and PVC ($|\Delta\delta|$), enabling direct assessment of their thermodynamic compatibility. Based on Hildebrand's theory, the enthalpy changes of mixing ΔH_v can be expressed as

$$\Delta H_m = V_0(\delta_1 - \delta_2)^2\phi_1\phi_2 = V_0|\Delta\delta|^2\phi_1\phi_2, \quad (7)$$

where V_0 is the volume of the mixture monomer, and ϕ_1 and ϕ_2 are the volume fractions of component 1 and 2, respectively. Therefore, the magnitude of $|\Delta\delta|$ serves as an indicator of the degree of miscibility between two components; a larger value suggests reduced compatibility due to heightened disparities in their cohesive energy densities. Empirical evidence suggests that two polymers are miscible provided that their solubility parameters are close enough, such as $(\delta_1 - \delta_2)^2 \leq 2.0$ MPa.[20] Fig. 4b illustrates the dependence of $|\Delta\delta|$ on chlorine content (Cl wt%) in CPEs. The $|\Delta\delta|$ is seen to decrease with increasing Cl wt%, suggesting enhanced CPE/PVC miscibility. r-CPE exhibits better compatibility with PVC compared to b-CPE. However, CPEs with <42.4 wt% Cl are indeed thermodynamically immiscible with PVC, as evidenced by the large $|\Delta\delta| \approx 0.98$ $MPa^{0.5}$ observed for r-CPE/PVC blends at 42.4 Cl wt%, together with the Flory–Huggins interaction parameter and phase diagram, which will be discussed later.

Table 4 Solubility parameters of CPE with varying chlorine contents

	δ_{CPE} ($MPa^{0.5}$)				
Cl wt%	b-CPE	r-CPE	δ_{PVC} ($MPa^{0.5}$)	$\lvert\Delta\delta_1\rvert^a$ ($MPa^{0.5}$)	$\lvert\Delta\delta_2\rvert^b$ ($MPa^{0.5}$)
26.9%	19.39	19.41	21.20	1.81	1.79
30.0%	19.46	19.55		1.74	1.65
32.9%	19.53	19.75		1.67	1.45
35.6%	19.62	19.88		1.58	1.32
38.0%	19.71	19.99		1.49	1.21
40.3%	19.94	20.33		1.26	0.87
42.4%	19.97	20.22		1.23	0.98

[a] $|\Delta\delta_1| = |\delta_{b\text{-}CPE} - \delta_{PVC}|$. [b] $|\Delta\delta_2| = |\delta_{r\text{-}CPE} - \delta_{PVC}|$.

3.1.2 Hansen solubility parameter. Actually, the Hilderbrand solubility parameter is most applicable to non-polar systems and may not adequately predict compatibility in blends involving highly polar or hydrogen-bonded polymers.[47] In this regard, we adopt the Hansen solubility parameter to determine the CPE/PVC miscibility, by taking the dispersion forces, polar forces, and hydrogen bonding forces into account. The Hansen solubility parameter is characterized by

$$\delta^2 = \delta_d{}^2 + \delta_p{}^2 + \delta_h{}^2, \quad (8)$$

where δ_d, δ_p, and δ_h represent the dispersion component, polar component, and hydrogen-bonding component, respectively. In our simulations, the non-bonded pairwise interactions can be divided into the van der Waals and the electrostatic parts (eqn (2)), allowing us to estimate the energy contributions from van der Waals (δ_{vdw}) and the electrostatic (δ_q) interactions separately. The solubility parameters calculated using Hansen method for CPE and PVC are summarized in Table 5. In this study, the van der Waals energy ($E_{van\ der\ Waals}$) and electrostatic energy ($E_{electrostatic}$) obtained from the COMPASS force field are used as quantitative descriptors of intermolecular interactions within an energy-decomposition framework. The van der Waals term, described by a Lennard-Jones 9-6 potential (eqn (3)), primarily reflects instantaneous dipole-induced dipole (dispersion) interactions and thus corresponds to the dispersive component (δ_d) of the Hansen solubility parameters. The electrostatic term (eqn (4)), computed using the Ewald summation method, represents permanent dipole–dipole interactions and captures the physical origins of the polar (δ_p) and hydrogen-bonding (δ_h) components. Given the negligible contribution of hydrogen bonding in the present system, δ_h can thus be reasonably omitted, such that $E_{van\ der\ Waals}$ and $E_{electrostatic}$ primarily correspond to δ_d and δ_p, respectively.

Fig. 5 illustrates the dependence of the Hansen solubility parameters on chlorine contents (Cl wt%). Notably, the van der Waals solubility parameters δ_{vdw} for both b-CPE and r-CPE exhibit minimal dependent on Cl wt%. Specifically, the δ_{vdw} of CPEs remains approximately 18.5 $MPa^{0.5}$, slightly lower than that of pure PVC, indicating comparable van der Waals contributions to intermolecular interactions. In contrast, the electrostatic solubility parameter δ_q of CPEs increases markedly and almost linearly with increasing Cl wt%. The δ_q of CPEs is seen to significantly lower than that of PVC (8.10 $MPa^{0.5}$), which accounts for the immiscibility behavior between CPE and PVC.

Furthermore, the solubility parameter for r-CPE demonstrates a greater sensitivity to Cl wt% compared to b-CPE, as evidenced by the relationships for δ_q in r-CPE ($\delta_q \propto 0.161$ Cl wt%) and b-CPE ($\delta_q \propto 0.131$ Cl wt%). As shown in Fig. 5d, the difference in δ_q between CPE and PVC decreases substantially with increasing Cl wt%, contributing to the enhanced CPE/PVC miscibility discussed in Section 3.1. It can thus be inferred that the solubility parameters of chlorine-containing vinyl polymers are crucially dependent on their chlorine content and the chlorine distribution, owing to the significant contributions from polar electrostatic interactions.

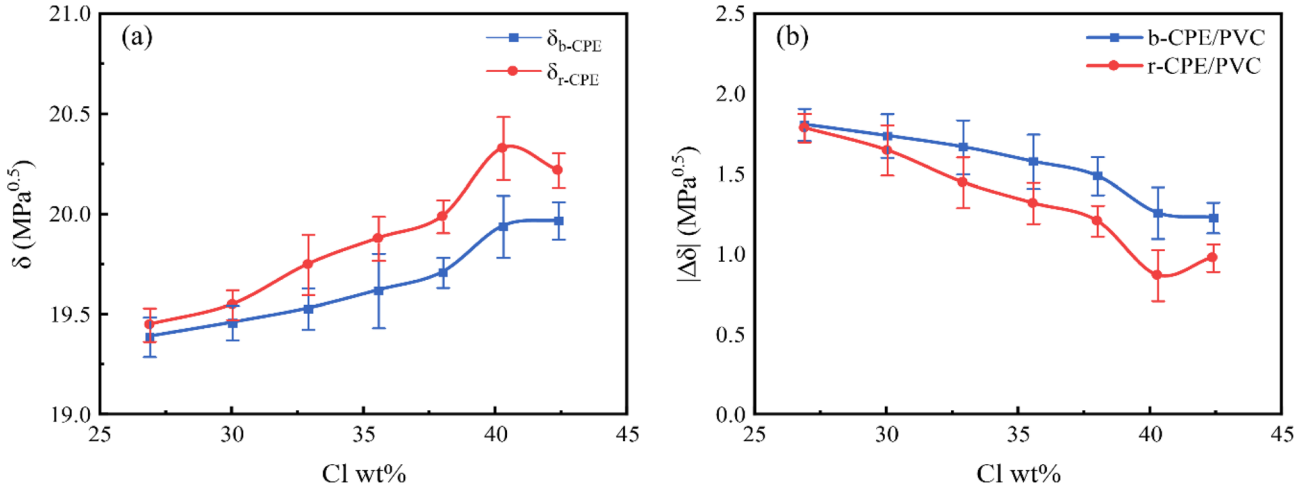

Fig. 4 Changes in (a) solubility parameter (δ) and (b) solubility parameter difference ($|\Delta\delta|$) as a function of chlorine contents (Cl wt%).

3.2 Effects of CPE/PVC blend composition

3.2.1 Solubility parameter. We now investigate the effects of blend composition on CPE/PVC blend miscibility by keeping chlorine content of r-CPE fixed at 35.6 Cl wt%. Seven blend ratios were systematically prepared to isolate the effects of composition, as detailed in Table 2. The obtained results of Hildebrand solubility parameters (δ), and its van der Waals

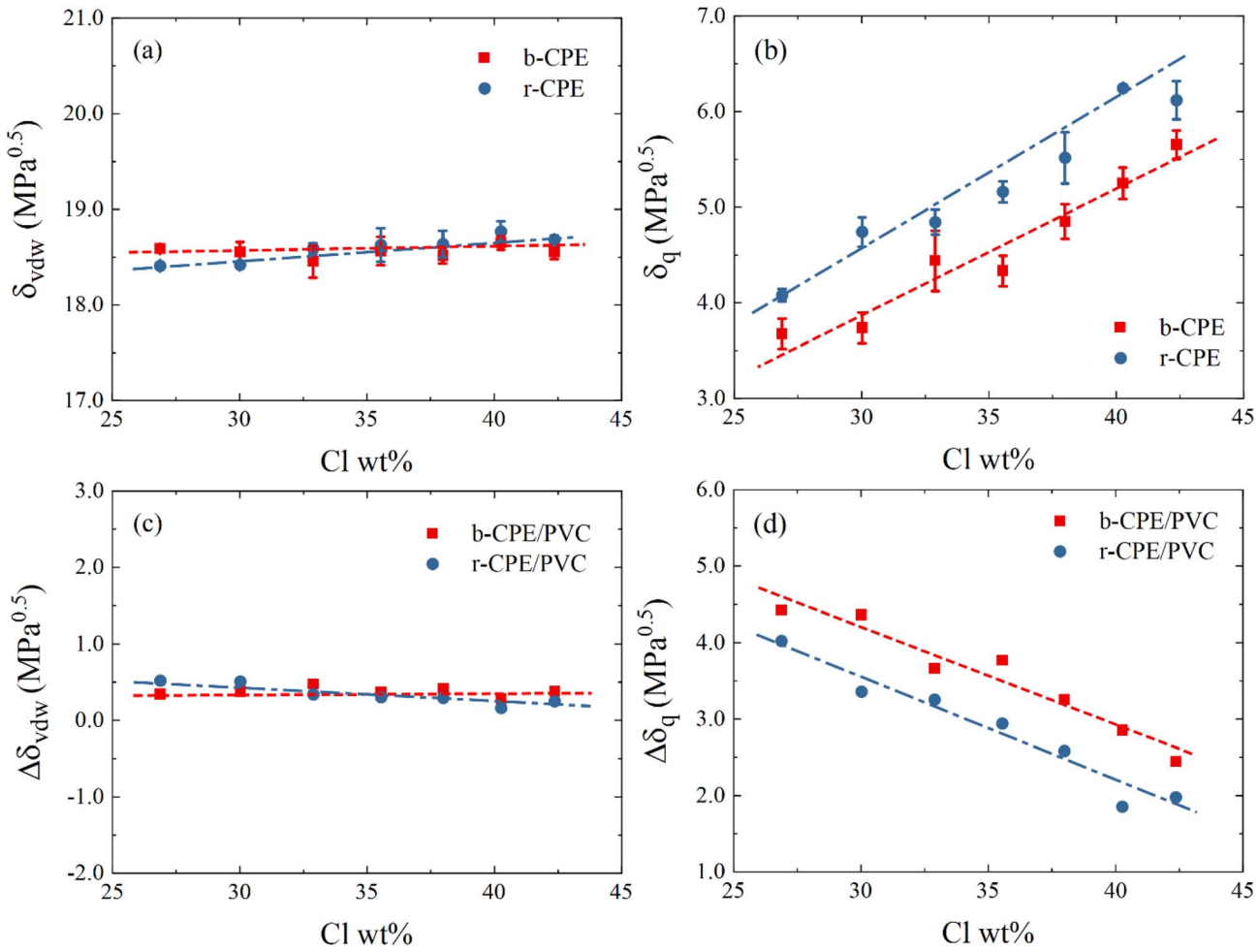

Fig. 5 Influences of chlorine contents (Cl%) on (a) van der Waals and (b) electrostatic contributions to solubility parameter (δ), and (c) van der Waals and (d) electrostatic solubility parameter difference ($\Delta\delta$).

Table 5 Hansen solubility parameters for CPE and PVC

	δ_{vdw} (MPa$^{0.5}$)			δ_q (MPa$^{0.5}$)		
Cl wt%	PVC	b-CPE	r-CPE	PVC	b-CPE	r-CPE
26.9%	18.93	18.58	18.41	8.10	3.68	4.08
30.0%		18.55	18.42		3.74	4.74
32.9%		18.45	18.59		4.43	4.84
35.6%		18.56	18.63		4.33	5.16
38.0%		18.51	18.64		4.85	5.52
40.3%		18.65	18.78		5.25	6.24
42.4%		18.55	18.68		5.65	6.12

interaction (δ_{vdw}) and electrostatic interaction (δ_q) components are tabulated in Table 6.

Fig. 6 presents the composition dependence of solubility parameters for CPE/PVC blends. It can be found that the Hildebrand solubility parameter δ is decreased with increasing CPE wt% in a modest behavior. This trend primarily reflects the behavior of the electrostatic component (δ_q), which decreases significantly with increasing CPE content, consistent with our earlier findings highlighting the chlorine-mediated intermolecular interactions in chlorine-containing vinyl polymers. In contrast, the van der Waals component (δ_{vdw}) shows negligible compositional dependence.

Notably, the electrostatic solubility parameter δ_q demonstrates a distinct upturn at CPE concentrations above ~80 wt%, suggesting enhanced blend compatibility in this regime. We attribute this behavior to intensified polar Cl–Cl interactions between dispersed PVC chains within the CPE matrix. This interpretation is further supported by the free energy analysis and phase behavior presented in Section 3.3, which confirms improved miscibility at high CPE loadings.

3.2.2 Flory–Huggins interaction parameter. To quantitatively assess the miscibility of the CPE/PVC blend, we evaluate the Flory–Huggins interaction parameter (χ_{12}), a key thermodynamic indicator of polymer–polymer compatibility.[48] The χ_{12} parameter measures the excess free energy of mixing and thus describes the phase behavior in polymer mixtures.[45] The Flory–Huggins parameter (χ_{12}) is obtained *via*:

$$\chi_{12} = \frac{z\Delta E_{mix}}{RT}, \quad (9)$$

where the coordination number z is equal to 6 for a cubic lattice model, and ΔE_{mix} is the mixing energy of polymer blend. For

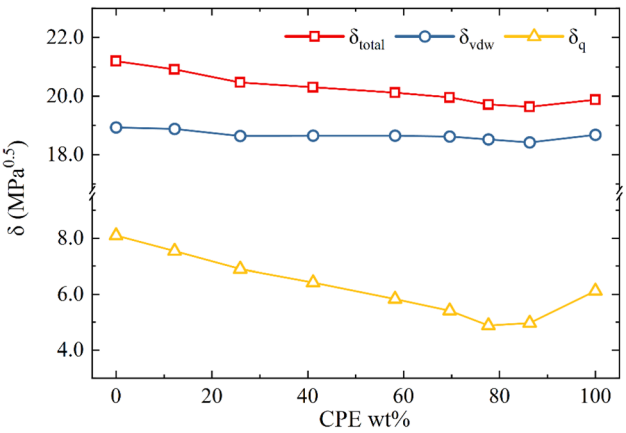

Fig. 6 Solubility parameters of CPE/PVC blends as a function of CPE content (CPE wt%).

a binary system (CPE/PVC), the mixing energy ΔE_{mix} is given by

$$\Delta E_{mix} = \phi_A \left(\frac{E_{coh}}{V}\right)_A + \phi_B \left(\frac{E_{coh}}{V}\right)_B - \left(\frac{E_{coh}}{V}\right)_{mix}. \quad (10)$$

Here, the subscripts *A*, *B*, and mix denote CPE, PVC, and their blend, respectively; ϕ_A and ϕ_B are the volume fractions of the two polymers. The calculated Flory–Huggins interaction parameters for CPE/PVC blends are given in Table 7.

In theory, lower (negative) χ_{12} values indicate favorable miscibility, whereas higher values denote thermodynamic incompatibility and a propensity for phase separation. To predict the miscibility of polymer blends more accurately, the critical Flory–Huggins parameter, χ_{cr}, is calculated as follows,

$$\chi_{cr} = \frac{1}{2}\left(\frac{1}{\sqrt{n_A}} + \frac{1}{\sqrt{n_B}}\right)^2, \quad (11)$$

where n_A and n_B represent the degree of polymerization for polymers A and B, respectively. Assuming segmental-level mixing, corresponding to monomer size in this study. A polymer blend is predicted to be miscible if its χ_{12} parameter is lower than χ_{cr}; conversely, immiscibility is expected if $\chi_{12} > \chi_{cr}$. Partial miscibility exists when χ_{12} is marginally greater than χ_{cr}. In this work, both CPE and PVC are assigned a degree of polymerization of 20, yielding a χ_{cr} value of 0.15.

Fig. 7 illustrates the calculated χ_{12} parameters of CPE/PVC blends as a function of CPE content. It is evident that the χ_{12}

Table 6 Solubility parameters for CPE/PVC blends

CPE wt%	δ (MPa$^{0.5}$)	δ_{vdw} (MPa$^{0.5}$)	δ_q (MPa$^{0.5}$)
0%	21.20	18.93	8.10
12.2%	20.92	18.88	7.54
25.9%	20.47	18.64	6.90
41.1%	20.31	18.65	6.42
58.2%	20.12	18.65	5.83
69.6%	19.96	18.62	5.41
77.7%	19.72	18.52	4.88
86.3%	19.64	18.42	4.97
100%	19.88	18.68	6.12

Table 7 Flory–Huggins interaction parameters for CPE/PVC blends

CPE wt%	χ_{12}	χ_{cr}
12.2%	0.07	0.15
25.9%	0.27	0.15
41.1%	0.22	0.15
58.2%	0.18	0.15
69.6%	0.17	0.15
77.7%	0.26	0.15
86.3%	0.13	0.15

values of polymer blends with approximately 20–80 wt% CPE lie above the critical χ_{cr} line, indicating immiscible behavior. Specifically, when CPE content ranges from approximately 60–80 wt%, the χ_{12} values are seen to be slightly larger than χ_{cr}, potentially suggesting partial miscibility of the CPE/PVC blends. Furthermore, as anticipated, CPE/PVC blends with a predominant proportion of either CPE or PVC (*i.e.*, close to the pure polymer) exhibit miscibility, as evidenced by their relatively small χ_{12} values, which fall below χ_{cr} in Fig. 7.

3.3 Effects of temperature

3.3.1 Solubility parameter. We now examine the temperature dependence of miscibility in CPE/PVC blends by analyzing systems with a fixed chlorine content of 35.6% in CPE. The solubility parameters are calculated across temperatures ranging from 250 K to 450 K, spanning both glassy and rubbery regimes of PVC ($T_g \approx 370$ K). The solubility parameters (δ) of CPE and PVC, along with their difference ($\Delta\delta$) are summarized in Table 8.

As illustrated in Fig. 8, which plots solubility parameters against blending temperature, both PVC and CPE exhibit a marked decrease in δ with increasing temperature. Specifically, the solubility parameter for both b-CPE and r-CPE shows an almost linear decrease with temperature. This observation aligns well with earlier work on the temperature dependence of solubility parameters for amorphous polymers.[49,50]

Within the framework of free volume theory, the temperature dependence of solubility parameters can be described by two distinct regimes.[51,52] Below the glass transition temperature (T_g), the solubility parameter δ can be described by:

$$\delta(T) = \alpha_g(T - T_g) + \delta_g, \quad (12)$$

where δ_g represents the solubility parameter at T_g and α_g is the thermal coefficient of δ in the glassy state. Above T_g in the rubbery regime, the temperature dependence of δ is governed by

$$\delta(T) = \alpha_r(T - T_g) + \delta_g, \quad (13)$$

where α_r denotes the thermal coefficient in the rubbery state. Given that CPEs typically exhibit T_g values near or below 250 K, it is likely that the glass transition region for these materials falls outside our measurement window in Fig. 8a. Consequently, we apply linear regression using eqn (13) to determine the temperature dependence of δ and the corresponding thermal coefficients in the rubbery state. For b-CPE, the resulting relationship is given by

$$\delta(T) = -0.0023 \times T + 20.85, \quad (14)$$

yielding a thermal coefficient of -0.0023 ($MPa^{0.5}$ T^{-1}). For r-CPE, the relationship follows

$$\delta(T) = -0.0032 \times T + 21.32, \quad (15)$$

corresponding to a thermal coefficient of -0.0032 ($MPa^{0.5}$ T^{-1}). This observation suggests that r-CPE exhibits a stronger temperature dependence in terms of its solubility parameter in the rubbery state. Such a finding aligns well with our earlier interpretation regarding weaker interchain dipole–dipole interactions mediated by chlorine atoms in b-CPE, leading to less sensitivity of its solubility characteristics to temperature variations. Within the temperature range investigated in this study, the solubility parameter of PVC exhibits an abrupt change at approximately 370 K, which is indicative of its glass transition temperature ($T_g \approx 370$ K). This allows us to analyze the temperature dependence in two distinct regimes. It should be mentioned that the simulated T_g of PVC is slightly higher than experimental values reported in the literature ($\approx$338–352 K),[53,54] with a deviation of approximately 20 K. The observed discrepancy can be primarily ascribed to the simplified force-fields and much shorter simulation time scales relative to real experimental systems,[55–57] and the indirect determination of T_g based on solubility parameter analysis in the simulation model. By applying eqn (12) and (13) to the respective temperature ranges, we then obtain the following relations:

for $T \leq T_g$,

$$\delta(T) = -0.00069 \times (T - 370.03) + 21.19 \quad (16)$$

for $T \geq T_g$,

$$\delta(T) = -0.0027 \times (T - 370.03) + 22.19 \quad (17)$$

These expressions predict thermal expansion coefficients of solubility parameter equal to -0.00069 ($MPa^{0.5}$ T^{-1}) in the glassy state and -0.0027 ($MPa^{0.5}$ T^{-1}) in the rubbery state, indicating a significantly enhanced temperature sensitivity above T_g. Although the thermal expansion coefficients (α) reported here are derived from the temperature dependence of solubility parameter $\delta(T)$, with no direct experimental validation of α performed, the predicted values and their qualitative behavior should be physically reasonable and indeed consistent with established literature[58,59] on PVC.

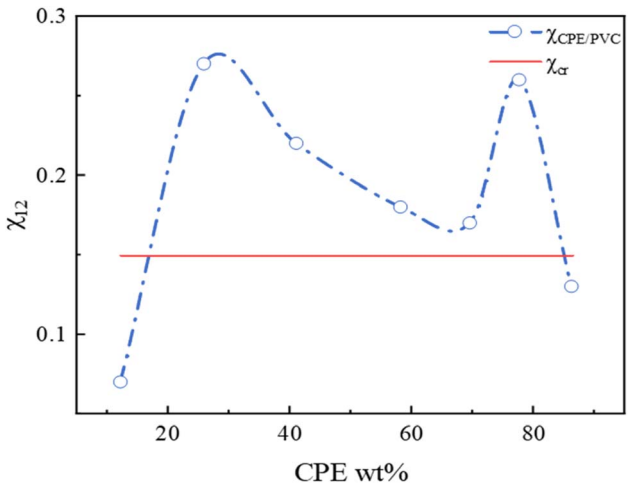

Fig. 7 Flory–Huggins interaction parameters (χ_{12}) *versus* CPE content (CPE wt%).

Table 8 Solubility parameters and Flory–Huggins interactions parameters of PVC and CPE

T (K)	δ_{PVC} (MPa$^{0.5}$)	$\delta_{b\text{-}CPE}$ (MPa$^{0.5}$)	$\delta_{r\text{-}CPE}$ (MPa$^{0.5}$)	$\lvert\Delta\delta_1\rvert^a$ (MPa$^{0.5}$)	$\lvert\Delta\delta_2\rvert^b$ (MPa$^{0.5}$)	χ_{12} of b-CPE/PVC	χ_{12} of r-CPE/PVC
250	21.18	20.31	20.48	0.87	0.70	0.21	0.13
300	21.26	20.13	20.31	1.13	0.95	0.34	0.24
350	21.24	20.18	20.27	1.06	0.97	0.31	0.25
400	21.18	19.92	20.17	1.26	1.01	0.43	0.28
450	20.96	19.81	19.80	1.15	1.14	0.36	0.35

^{a} $|\Delta\delta_1| = |\delta_{b\text{-}CPE} - \delta_{PVC}|$. ^{b} $|\Delta\delta_2| = |\delta_{r\text{-}CPE} - \delta_{PVC}|$.

Furthermore, as shown in Fig. 8b, the difference in solubility parameters ($\Delta\delta$) between CPE and PVC increase substantially with rising temperature, suggesting a remarkable reduction in the miscibility of the CPE/PVC blend. Notably, under identical thermal conditions, r-CPE demonstrates superior compatibility with PVC compared to b-CPE across the entire temperature ranged studied, as evidenced by consistently lower $\Delta\delta$ values.

3.3.2 Flory–Huggins interaction parameter. We now turn to investigate the influence of blending temperature on the Flory–Huggins interaction parameters (χ_{12}). For unfavorably/partially miscible blending systems where $\chi_{12} > 0$, the interaction parameter χ_{12} can be estimated from the solubility parameters of the constituent polymers by combining eqn (7) and (9), leading to the expression:

$$\chi_{12} = \frac{V_0}{k_B T}(\delta_1 - \delta_2)^2, \quad (18)$$

where V_0 is the average volume of repeating units, assuming comparable segment sizes for both polymers, and k_B is the Boltzmann constant. In our modeled CPE/PVC composites, the average Kuhn length of repeating units is approximately 7.3 Å, corresponding to an average segment volume of $V_0 \approx 203.7$ Å^3. The calculated χ_{12} are presented in Table 8 and illustrated in Fig. 9.

Fig. 9a presents the Flory–Huggins interaction parameters (χ_{12}) for CPE/PVC blends as a function of temperature. Both b-CPE/PVC and r-CPE/PVC blends exhibit increasing χ_{12} values with rising temperature, indicting a progressive decline in miscibility. This behavior can be attributed to the enhanced molecular motion at higher temperatures, which intensifies chain mobility and softens the polymer chains, thereby weakening intermolecular electrostatic interactions and diminishing the compatibility between the CPE and PVC components.

Notably, at the lowest examined temperature of 250 K, the value for the r-CPE/PVC blend falls below the critical threshold of the Flory–Huggins parameter line ($\chi_{cr} = 0.15$), suggesting the onset of miscibility under such conditions.

The temperature dependence of χ_{12} can be reliably described by the following equation:[60,61]

$$\chi_{12} \simeq A + \frac{B}{T}, \quad (19)$$

where the constants A and B denote the entropic and enthalpic contributions to χ_{12}, respectively.[47] By applying eqn (19) to our simulation data (Table 8), we obtain the best-fit temperature dependence of χ_{12}, as indicted by the straight lines in Fig. 9b:

For b-CPE/PVC blend,

$$\chi_{12} = -\frac{94.28}{T} + 0.6112 \quad (20)$$

For r-CPE/PVC blend,

$$\chi_{12} = -\frac{108.88}{T} + 0.5747 \quad (21)$$

According to the results, a homogenous phase is expected to emerge upon cooling for both CPE/PVC blends, given that $A >$

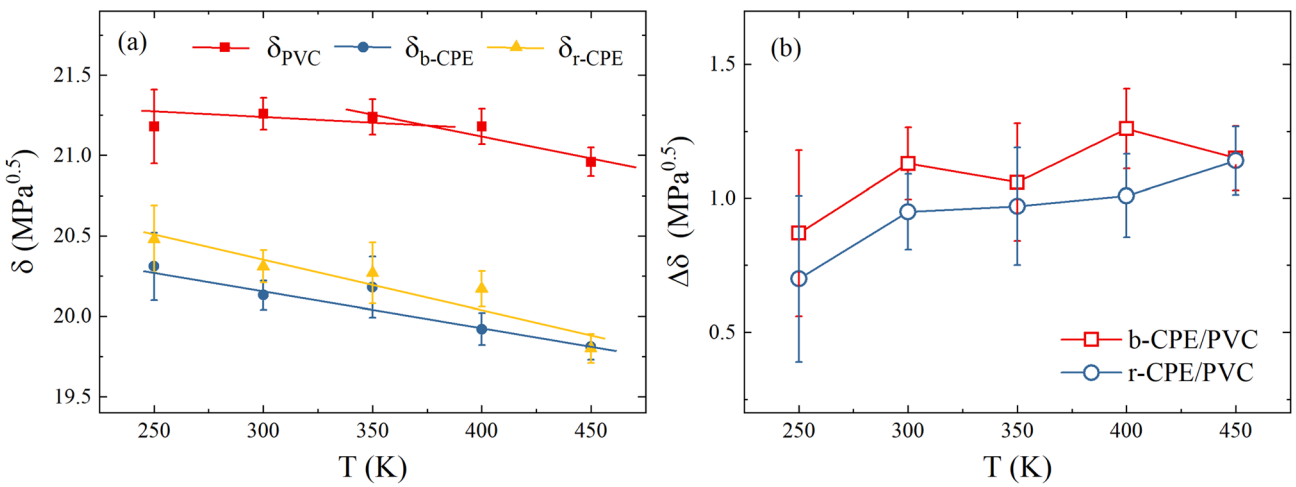

Fig. 8 (a) Solubility parameter (δ) and (b) solubility parameter difference ($|\Delta\delta|$) as a function of blending temperature.

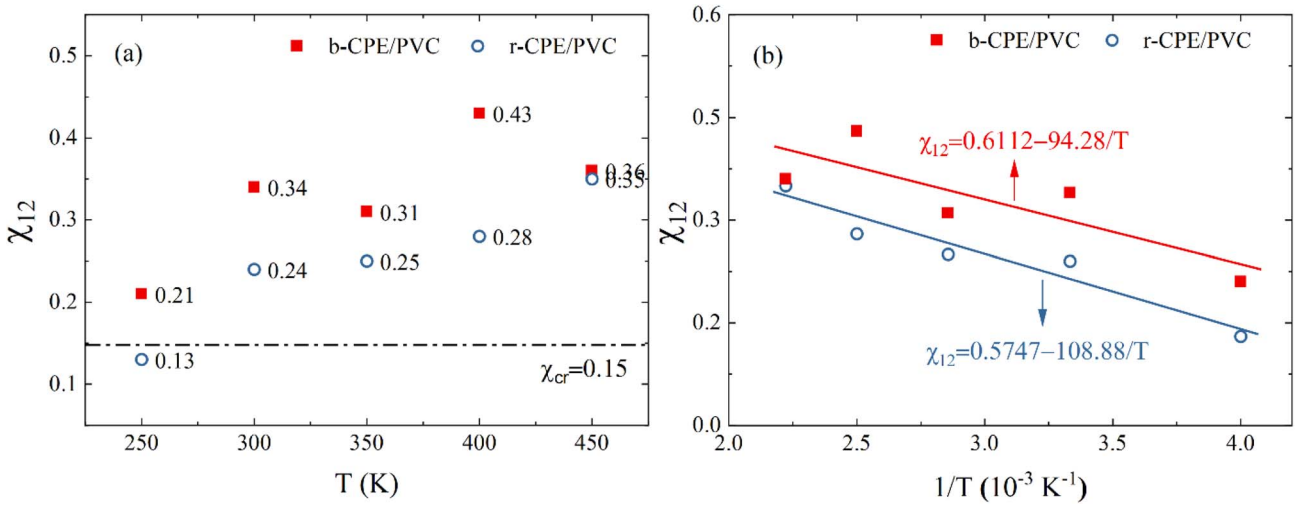

Fig. 9 Temperature dependence of Flory–Huggins interaction parameters (χ_{12}) for CPE/PVC blends with CPEs containing 35.6 wt% chlorine: (a) χ_{12} as a function of temperature (T), and (b) χ_{12} *versus* reciprocal temperature ($1/T$) for the application of eqn (19).

0 and $B < 0$. However, the phase behavior of r-CPE/PVC blends is found to be more sensitive to blending temperature compared to that of b-CPE/PVC blends.

3.4 Phase diagram analysis

3.4.1 Free energy of mixing. With the established temperature dependence of χ_{12}, it is now possible to evaluate the free energy and thereby predict the miscibility behavior of CPE/PVC blends by applying the classical Flory–Huggins theory of mixing.[62] The molar free energy of mixing (ΔF_{mix}) is given by

$$\frac{\Delta F_{mix}}{RT} = \frac{\phi_A}{n_A}\ln \phi_A + \frac{\phi_B}{n_B}\ln \phi_B + \chi\phi_A\phi_B, \quad (22)$$

where the first two terms represent the entropic contribution, and the third term arises from the energetic (enthalpic) interactions. Negative values of ΔF_{mix} indicate thermodynamically favorable miscibility, whereas positive values signify phase separation. By incorporating the temperature dependence of χ_{12} (as described by eqn (20) and (21)) into eqn (22), we compute the molar free energy of mixing for CPE/PVC blends across a range of temperatures as a function of the volume fraction of CPE. The results are depicted in Fig. 10.

For our simulated CPE/PVC models with equal chain lengths ($n_A = n_B = 20$), the free energy curves exhibit symmetric profiles. As the temperature decreases, the free energy of mixing transitions from positive into negative values, indicating enhanced compatibility. Since the entropic contribution always increases with temperature, the observed improvement in CPE/PVC miscibility at lower temperatures must be attributed to the enthalpic component, reflecting the growing significance of attractive chlorine-mediated intermolecular interactions.

Moreover, the free energy curves evolve from convex to concave shapes at sufficiently low temperatures (*e.g.*, 150 K for b-CPE/PVC blend or 200 K for r-CPE/PVC blend), implying that all blend compositions are thermodynamically stable, as indicated by a negative second derivative of the free energy of mixing. Actually, this scenario corresponds to values of Flory–Huggins interaction parameters than fall below the critical threshold ($\chi_{12} < \chi_{cr}$). By the way, the Gibbs free energy may overestimate the miscibility (χ_{12}) for non-polar polymers.[33]

3.4.2 Phase diagram of blends. As discussed above, the free energy of mixing for binary CPE/PVC systems exhibits a convex shape at high temperatures, indicative of thermodynamic instability, while adopting a concave form at low temperatures, corresponding to stable mixing. At certain intermediate temperatures, *e.g.*, 200 K for the b-CPE/PVC blend and 250 K for the r-CPE/PVC blend, the free energy curves display more complex behavior: two concave segments in regions rich in either CPE or PVC, separate by a convex segment in the intermediate composition range, as shown in Fig. 11. To provide a more detailed characterization of these features, phase diagrams delineating stable and unstable regimes have been computed. The local stability of the mixture can be accessed by examining the second derivative of free energy of mixing with respect to composition:

$$\frac{\partial^2 \Delta F_{mix}}{\partial \phi_A{}^2} = RT\left(\frac{1}{n_A\phi_A} + \frac{1}{n_B\phi_B} - 2\chi_{12}\right), \quad (23)$$

where a negative value implies a tendency towards spontaneous phase separation (spinodal decomposition), while a positive value indicates a locally stable equilibrium. Accordingly, the spinodal decomposition curve, defined by the condition $\frac{\partial^2 \Delta F_{mix}}{\partial \phi_A{}^2} = 0$, is determined and depicted as the dashed red curve in Fig. 11. Within this region, slight fluctuations in composition will grow spontaneously, leading to phase separation without an energy barrier.

However, phase separations *via* binodal mechanisms (nucleation and growth) may also occur within the locally stable regime where the second derivative of free energy of mixing is positive $\left(\frac{\partial^2 \Delta F_{mix}}{\partial \phi_A{}^2} > 0\right)$ if composition fluctuations is

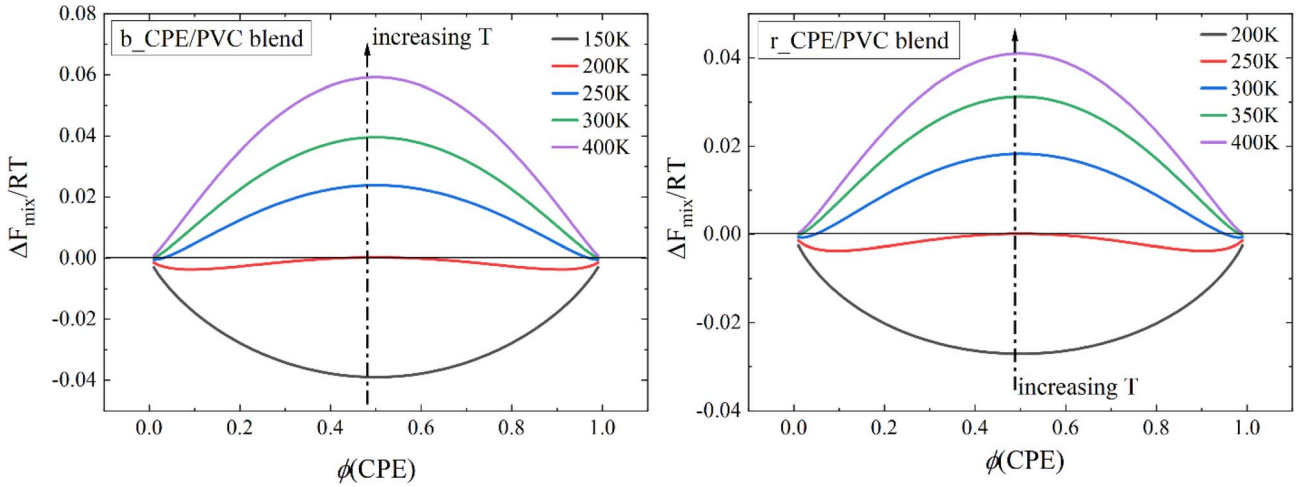

Fig. 10 Free energy of mixing for CPE/PVC blends as a function of mole fraction of CPE.

sufficiently large to nucleate a new phase (a domain of critical size). The binodal curve, which marks the boundary between coexisting phases, is determined by the condition that the first derivative of free energy of mixing is equal to zero:

$$\frac{\partial \Delta F_{\text{mix}}}{\partial \phi_{\text{A}}} = RT\left[\frac{1+\ln \phi_{\text{A}}}{n_{\text{A}}} - \frac{1+\ln \phi_{\text{B}}}{n_{\text{B}}} + \chi_{12}(1-2\phi_{\text{A}})\right]. \quad (24)$$

The binodal curve is plotted as the solid black line in the phase diagram (Fig. 12). Consequently, the region bounded by the binodal and spinodal curves corresponds to the metastable regime, where phase separation may proceed *via* nucleation-driven processes.

As shown in Fig. 11, both CPE/PVC binary systems exhibit a lower critical solution temperature (LCST) behavior, consistent with the earlier observations derived from the solubility parameters and Flory–Huggins interaction parameters. Specifically, CPE/PVC blends of certain compositions may undergo phase separation into two phases at elevated temperatures, while upon cooling, they form a single, thermodynamically stable phase.

Below the LCST temperature (T_{cr}), the CPE/PVC systems can be prepared as stable homogenous mixtures across all compositions. For our simulated CPE/PVC systems, the b-CPE/PVC blends exhibit a T_{cr} of approximately 184.43 K, while r-CPE/PVC blends show a higher T_{cr} of approximately 229.36 K. These results indicate that the r-CPE demonstrates superior miscibility with PVC compared to b-CPE under identical conditions of temperature and blend composition.

To provide a direct validation of the calculated phase diagram, the simulation snapshots corresponding to $T = 300$ K and $T = 160$ K for the r-CPE/PVC system (at 35.6 wt% Cl and 58.2 wt% CPE) are further compared in Fig. 12. It can be seen that at the higher temperature of 300 K within the two-phase region of the phase diagram (Fig. 11b), the r-CPE and PVC chains are clearly segregated into aggregated domains, demonstrating the phase separation. In contrast, at the temperature of 160 K below the LCST temperature T_{cr}, the

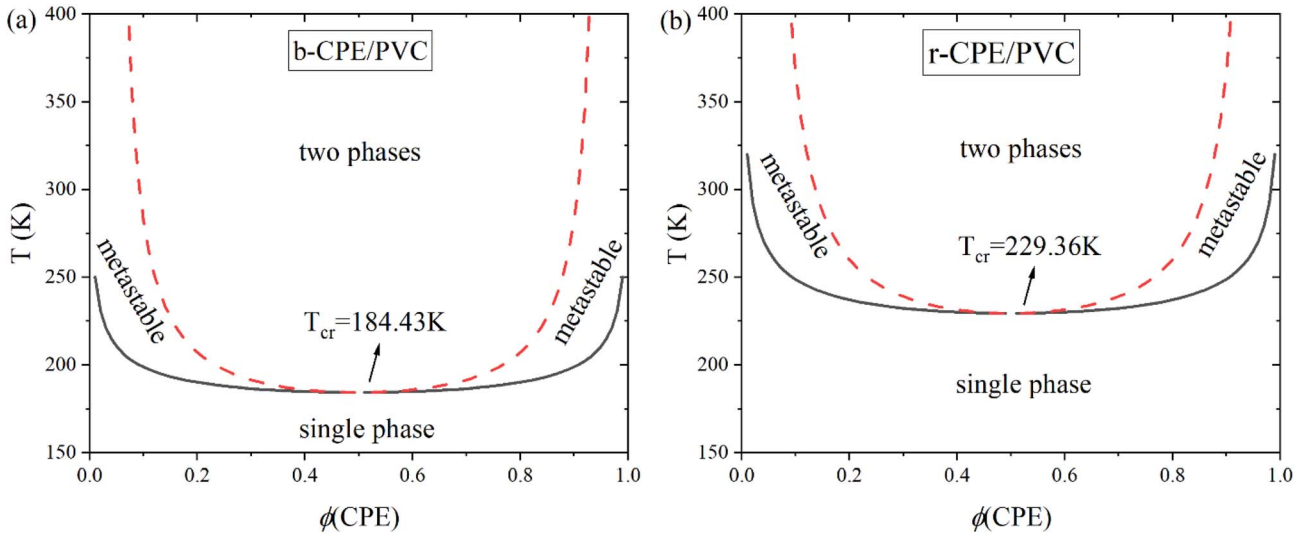

Fig. 11 Phase diagram of (a) b-CPE/PVC and (b) r-CPE/PVC blends.

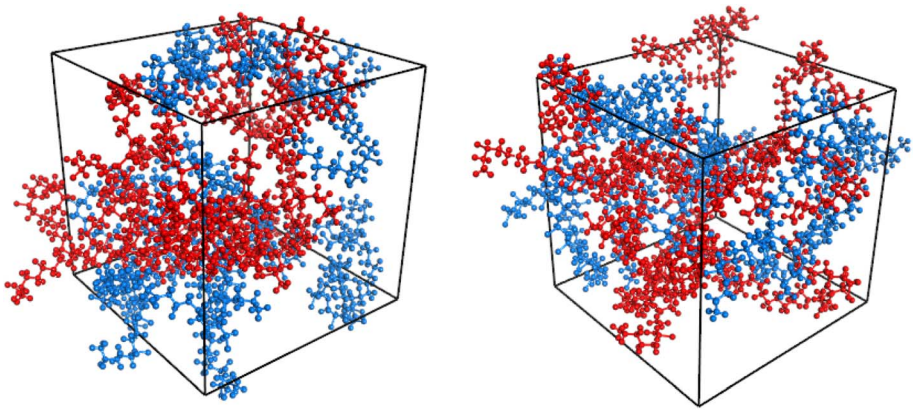

Fig. 12 Representative equilibrium snapshots of the r-CPE/PVC blend with 58.2 wt% r-CPE (35.6 wt% Cl) at (a) 300 K and (b) 160 K. The PVC chains are rendered in blue, and the r-CPE chains in red.

polymer chains are observed to be more dispersed across the whole simulation box, indicating the well-mixed state. Such phenomenon is consistent with the LCST behavior previously identified for the CPE/PVC blend system, and thus directly corroborates the validity of our predicted phase diagrams shown in Fig. 11.

4 Conclusion

In this study, all-atom molecular dynamics simulations are employed to systematically investigate the effects of CPE chlorine content, molecular architecture, blend composition, and temperature on the miscibility of CPE/PVC binary systems. CPE chains with varying chlorine contents (Cl wt%) and distinct structural configurations—characterized by random *versus* block distributions of Cl atoms—are considered. The blend miscibility behavior is characterized using Hildebrand and Hansen solubility parameters (δ), Flory–Huggins interaction parameters (χ_{12}) and phase diagrams. The simulation results reveal that the overall δ for both CPEs are increased with Cl wt% within the investigated range. Such a trend is primary driven by electrostatic interactions (δ_q) arising from polar Cl–Cl interactions, while the van der Waals contributions (δ_{vdw}) remains largely independent of Cl wt%. Compared to b-CPE, r-CPE exhibits higher values of δ_{vdw} and consequently larger Hildebrand δ, which is mainly attributed to the fact that in b-CPE, polar –CH_2–CHCl– segments tend to segregate from nonpolar –CH_2–CH_2– units, thereby reducing interchain dipole–dipole interactions mediated by Cl atoms. Moreover, the dependence of χ_{12} on Cl wt% suggests that polymer blends containing approximately 20–80 wt% CPE are thermodynamically immiscible at 300 K, as demonstrated by the χ_{12} values falling below the critical miscibility threshold ($\chi_{cr} = 0.15$ in the present simulations), whereas CPE/PVC blends with a predominant proportion of either CPE or PVC exhibit miscibility. The δ for both CPEs and PVC are found to decrease with increasing temperature.

Our simulation results also demonstrate that the χ_{12} of CPE/PVC blends increase with temperature (T), indicating reduced miscibility at elevated temperatures. A quantitative χ_{12}–T relationship is established, revealing that the phase behavior of r-CPE/PVC blends is more sensitive to temperature changes than that of b-CPE/PVC blends. The free energy of mixing is also computed, showing that both CPE/PVC systems undergo a transition from convex to concave profile upon cooling, further supporting the enhanced CPE/PVC miscibility at lower temperatures. Phase diagrams confirm that CPE/PVC binary systems exhibit a low critical solution temperature (LCST) behavior, delineating the binodal and spinodal decomposition curves along with the associated metastable region. Notably, the r-CPE/PVC system displays a higher critical temperature of $T_{cr} \simeq 229.36$ K, compared to b-CPE/PVC blend with $T_{cr} \simeq 184.43$ K. Our simulation results show good agreement with experimental data regarding polymer density and solubility parameters, validating the accuracy of our simulation model, forcefield and computational methodology. In conclusion, we believe that our simulation work provides a comprehensive understanding of these factors governing CPE/PVC miscibility and offers valuable guidance for the design and fabrication of CPE/PVC composite materials.

Author contributions

Zhihao Ma: methodology, investigation, simulation, data collection, analysis, and writing – original draft; Xue Li: validation, supervision, and funding acquisition; Huaguo Xu: formal analysis and validation; Jianxiang Shen: conceptualization, supervision, project administration, funding acquisition, and writing – review & editing; Jun Liu: conceptualization, formal analysis, and validation.

Conflicts of interest

The authors declare no competing interest.

Data availability

The data that support the findings of this study are available on request from the corresponding author. The data are not publicly available due to privacy or ethical restrictions.

Acknowledgements

This work is financially supported by the National Natural Science Foundation of Zhejiang Province, China (LY24E030001), the National Natural Science Foundation of China (52203091), the Science and Technology Research Projects of Jiaxing City, Zhejiang Province (2024AY10046), the opening Foundation of State Key Laboratory of Organic–Inorganic Composites, Beijing University of Chemical Technology (oic-202401009), and Jiaxing University Graduate Research, Practice, and Innovation Program (PSRPIP2024003C). Computations were performed at the Wuzhen Supercomputer Center of China.

References

1 A. Al Alshaikh and J. E. Bara, Chlorinated plastics offer unique opportunities and challenges in upcycling, *Polym. Int.*, 2024, **73**(5), 341–348.
2 Y. Saeki and T. Emura, Technical progresses for PVC production, *Prog. Polym. Sci.*, 2002, **27**(10), 2055–2131.
3 A. K. Hussein, E. Yousif, M. K. Rasheed, G. I. Edo, M. Bufaroosha and H. Umar, Synthesis, Modification, and Applications of Poly(vinyl chloride) (PVC), *Polym.-Plast. Technol. Mater.*, 2024, **64**(5), 593–632.
4 G. I. Edo, W. Ndudi, A. B. M. Ali, E. Yousif, K. Zainulabdeen, P. N. Onyibe, H. A. Ekokotu, E. F. Isoje, U. A. Igbuku, A. E. A. Essaghah, D. S. Ahmed, H. Umar and D. U. Ozsahin, Poly(vinyl chloride) (PVC): an updated review of its properties, polymerization, modification, recycling, and applications, *J. Mater. Sci.*, 2024, **59**(47), 21605–21648.
5 J. Leadbitter, PVC and sustainability, *Prog. Polym. Sci.*, 2002, **27**(10), 2197–2226.
6 K. Lewandowski and K. Skórczewska, A Brief Review of Poly(Vinyl Chloride) (PVC) Recycling, *Polymers*, 2022, **14**(15), 3035.
7 J. Chu, Y. Zhou, Y. Cai, X. Wang, C. Li and Q. Liu, Life-cycle greenhouse gas emissions and the associated carbon-peak strategies for PS, PVC, and ABS plastics in China, *Resour., Conserv. Recycl.*, 2022, **182**, 106295.
8 A. Alshaikh, S. Ezendu, D. Ryoo, P. S. Shinde, J. L. Anderson, T. Szilvási, P. A. Rupar and J. E. Bara, PVC Modification through Sequential Dehydrochlorination–Hydrogenation Reaction Cycles Facilitated *via* Fractionation by Green Solvents, *ACS Appl. Polym. Mater.*, 2024, **6**(16), 9656–9662.
9 P. W. Skelly, L. Li and R. Braslau, Internal plasticization of PVC, *Polym. Rev.*, 2021, **62**(3), 485–528.
10 M. Khaleghi, Investigation of thermal and mechanical properties of new nitrogen-rich organic based heat stabilizers for poly (vinyl chloride), *J. Thermoplast. Compos. Mater.*, 2024, **37**(4), 1480–1498.
11 J. Guo, Y. Li, S. Song, S. Tan, S. Zhao, L. Li and H. Wang, The effects of ACR/MAH ionic cross-linking on the cell morphology, mechanical properties, and dimensional stability of PVC foams, *Polym. Degrad. Stab.*, 2024, **229**, 110946.
12 P. R. Kubade and R. Senanayake, Studies on thermo-mechanical properties of HNTs filled ABS/PVC composites, *Mater. Today: Proc.*, 2022, **59**, 248–252.
13 P. R. Kubade and R. Senanayake, Thermo-mechanical properties of polyethyleneimine (PEI) modified HNTs filled ABS/PVC composites, *Mater. Today: Proc.*, 2022, **59**, 852–857.
14 Y. Komori, A. Taniguchi, H. Shibata, S. Goto and H. Saito, Partial Miscibility and Concentration Distribution of Two-Phase Blends of Crosslinked NBR and PVC, *Polymers*, 2023, **15**(6), 1383.
15 C. Thoral, G. Soulagnet, P.-O. Bussiere and S. Therias, Impact of photo- and thermooxidative ageing of NBR/PVC blends on the formation of cracks, *Polym. Degrad. Stab.*, 2024, **220**, 110633.
16 S. N. Maiti, U. K. Saroop and A. Misra, Studies on polyblends of poly(vinyl chloride) and acrylonitrile-butadiene-styrene terpolymer, *Polym. Eng. Sci.*, 1992, **32**(1), 27–35.
17 H.-R. Jung and W.-J. Lee, Electrochemical characteristics of electrospun poly(methyl methacrylate)/polyvinyl chloride as gel polymer electrolytes for lithium ion battery, *Electrochim. Acta*, 2011, **58**, 674–680.
18 C. Zhou, S. Wu, H. Liu and G. Wu, Effects of core-shell particle growth manners on morphologies and properties of poly(vinyl chloride)/(methyl methacrylate-butadiene-styrene) blends, *J. Vinyl Addit. Technol.*, 2016, **22**(1), 37–42.
19 L. Liu, M. Chen, R. J. Dai, S. L. Sun, C. Zhou, H. D. Yang and H. X. Zhang, Toughness and Transparency of Poly(vinyl chloride)/Methyl Methacrylate-Butadiene-Styrene Blends with Varied Shell Phase Composition of Core-Shell Theories, *Polym.-Plast. Technol. Eng.*, 2009, **48**(9), 953–957.
20 J. Li, S.-H. Jin, G.-C. Lan, Z.-S. Xu, L.-T. Wang, N. Wang and L.-J. Li, Research on the Glass Transition Temperature and Mechanical Properties of Poly(vinyl chloride)/Dioctyl Phthalate (PVC/DOP) Blends by Molecular Dynamics Simulations, *Chin. J. Polym. Sci.*, 2019, **37**(8), 834–840.
21 F. You, G. Chen, J. Zou, Z. Yang and S. Guo, The experimental results and simulation of temperature dependence of brittle-ductile transition in PVC/CPE blends and PVC/CPE/nano-$CaCO_3$ composites, *J. Appl. Polym. Sci.*, 2012, **123**(3), 1833–1842.
22 J. Mnyango, L. Bolo, B. Fouda-Mbanga, Z. Tywabi-Ngeva, Y. Nthwane, K. Pillay, P. Ndibewu and S. Hlangothi, Advances in Chlorinated Polyethylene: Properties, Applications, and Future Directions, *J. Appl. Polym. Sci.*, 2025, e57526.
23 B.-M. Quenum, P. Berticat and G. Vallet, Chlorinated Polyethylene. III. Relationships of Microstructure and Thermal Properties, *Polym. J.*, 1975, **7**(3), 300–311.

24 X. Xie, W. Li and Y. Wei, Effect of Blending Modification on Tensile Performance of CPE/PVC, *Adv. Mater. Res.*, 2011, 1732–1735.
25 D. R. Paul and C. E. Locke, Chlorinated polyethylene modification of blends derived from waste plastics Part I: Mechanical behavior, *Polym. Eng. Sci.*, 1973, **13**(3), 202–208.
26 Y. Zhang, C. Ding, N. Zhang, H. Li, Y. Zhang, B. Deng and Y. Zhang, Contributions of TCA-KTTO-modified quartz tailings and CPE toughener in PVC composites to enhance the mechanical-thermal performance, *Chem. Eng. J.*, 2024, **495**, 153166.
27 A. Ahmadi and J. J. Freire, Molecular dynamics simulation of miscibility in several polymer blends, *Polymer*, 2009, **50**(20), 4973–4978.
28 S. S. Jawalkar and T. M. Aminabhavi, Molecular modeling simulations and thermodynamic approaches to investigate compatibility/incompatibility of poly(l-lactide) and poly(vinyl alcohol) blends, *Polymer*, 2006, **47**(23), 8061–8071.
29 S. Patel, A. Lavasanifar and P. Choi, Application of Molecular Dynamics Simulation To Predict the Compatability between Water-Insoluble Drugs and Self-Associating Poly(ethylene oxide)-b-poly(ε-caprolactone) Block Copolymers, *Biomacromolecules*, 2008, **9**(11), 3014–3023.
30 I. Martinez de Arenaza, E. Meaurio, B. Coto and J.-R. Sarasua, Molecular dynamics modelling for the analysis and prediction of miscibility in polylactide/polyvinilphenol blends, *Polymer*, 2010, **51**(19), 4431–4438.
31 S. Jawalkar, R. V. Kothapalli, S. Halligudi, M. Sairam and T. Aminabhavi, Molecular Modeling Simulations to Predict Compatibility of Poly(vinyl alcohol) and Chitosan Blends: A Comparison with Experiments, *J. Phys. Chem. B*, 2007, **111**, 2431–2439.
32 S. S. Patnaik and R. Pachter, A molecular simulations study of the miscibility in binary mixtures of polymers and low molecular weight molecules, *Polymer*, 2002, **43**(2), 415–424.
33 G. P. Costa, S. R. Stoyanov, Q. Liu and P. Choi, Solubility of selected polymers in cyclohexane: comparison between Flory–Huggins interaction parameters calculated using three different molecular dynamics simulation approaches, *Phys. Chem. Chem. Phys.*, 2024, **26**(47), 29628–29639.
34 M. D. Hanwell, D. E. Curtis, D. C. Lonie, T. Vandermeersch, E. Zurek and G. R. Hutchison, Avogadro: an advanced semantic chemical editor, visualization, and analysis platform, *J. Cheminf.*, 2012, **4**(1), 17.
35 F. V. Olowookere, A. Al Alshaikh, J. E. Bara and C. H. Turner, Effects of chain length on the structure and dynamics of polyvinyl chloride during atomistic molecular dynamics simulations, *Mol. Simul.*, 2023, **49**(15), 1401–1412.
36 J.-C. Huang, Miscibility of PVC with chlorinated PE and chlorinated PVC, *Int. J. Polym. Mater.*, 2003, **52**(8), 673–683.
37 H. Sun, P. Ren and J. R. Fried, The COMPASS force field: parameterization and validation for phosphazenes, *Comput. Theor. Polym. Sci.*, 1998, **8**(1), 229–246.
38 S. Plimpton, Fast parallel algorithms for short-range molecular dynamics, *J. Comput. Phys.*, 1995, **117**(1), 1–19.
39 M. Hadipeykani, F. Aghadavoudi and D. Toghraie, A molecular dynamics simulation of the glass transition temperature and volumetric thermal expansion coefficient of thermoset polymer based epoxy nanocomposite reinforced by CNT: a statistical study, *Phys. A*, 2020, **546**, 123995.
40 J. Shen, X. Li, P. Li and B. Shentu, Exploring thermodynamic and structural properties of carbon nanotube/thermoplastic polyurethane nanocomposites from atomistic molecular dynamics simulations, *RSC Adv.*, 2023, **13**(30), 21080–21087.
41 J. Shen, X. Li, P. Li and B. Shentu, Structural and dynamical properties of thermoplastic polyurethane/fullerene nanocomposites: a molecular dynamics simulations study, *Phys. Chem. Chem. Phys.*, 2023, **25**(40), 27352–27363.
42 S. Nosé, A molecular dynamics method for simulations in the canonical ensemble, *Mol. Phys.*, 2002, **100**(1), 191–198.
43 H. C. Andersen, Molecular dynamics simulations at constant pressure and/or temperature, *J. Chem. Phys.*, 1980, **72**(4), 2384–2393.
44 E. Fekete and B. Pukánszky, Effect of molecular interactions on the miscibility and structure of polymer blends, *Eur. Polym. J.*, 2005, **41**(4), 727–736.
45 J.-C. Huang and R. D. Deanin, Multicomponent solubility parameters of poly (vinyl chloride) and poly (tetramethylene glycol), *Fluid Phase Equilib.*, 2005, **227**(1), 125–133.
46 C. M. Hansen in *Hansen Solubility Parameters : A User's Handbook*, 2nd edn, 2007.
47 D. P. Faasen, A. Jarray, H. J. Zandvliet, E. S. Kooij and W. Kwiecinski, Hansen solubility parameters obtained *via* molecular dynamics simulations as a route to predict siloxane surfactant adsorption, *J. Colloid Interface Sci.*, 2020, **575**, 326–336.
48 M. Rubinstein. and R. H. Colby, *Polymer Physics*, Oxford University Press, 2003.
49 G. P. Costa, P. Choi, S. R. Stoyanov and Q. Liu, The temperature dependence of the Hildebrand solubility parameters of selected hydrocarbon polymers and hydrocarbon solvents: a molecular dynamics investigation, *J. Mol. Model.*, 2024, **30**(7), 196.
50 X. Chen, C. Yuan, C. K. Wong and G. Zhang, Molecular modeling of temperature dependence of solubility parameters for amorphous polymers, *J. Mol. Model.*, 2012, **18**(6), 2333–2341.
51 K. Chee, Temperature dependence of solubility parameters of polymers, *Malays. J. Chem.*, 2005, **7**, 57–61.
52 N. Tanaka, Prediction of solubility parameter from thermal transition behaviour in polymers, *Polymer*, 1992, **33**(3), 623–626.
53 T. Sterzyński, J. Tomaszewska, J. Andrzejewski and K. Skorczewska, Evaluation of glass transition temperature of PVC/POSS nanocomposites, *Compos. Sci. Technol.*, 2015, **117**, 398–403.
54 T. Sterzyński, J. Tomaszewska, K. Piszczek and K. Skórczewska, The influence of carbon nanotubes on the PVC glass transition temperature, *Compos. Sci. Technol.*, 2010, **70**(6), 966–969.
55 A. F. Behbahani, S. M. Vaez Allaei, G. H. Motlagh, H. Eslami and V. A. Harmandaris, Structure, dynamics, and apparent

glass transition of stereoregular poly (methyl methacrylate)/graphene interfaces through atomistic simulations, *Macromolecules*, 2018, **51**(19), 7518–7532.

56 A. Soldera and N. Metatla, Glass transition of polymers: Atomistic simulation *versus* experiments, *Phys. Rev. E: Stat., Nonlinear, Soft Matter Phys.*, 2006, **74**(6), 061803.

57 N. Metatla and A. Soldera, Computation of densities, bulk moduli and glass transition temperatures of vinylic polymers from atomistic simulation, *Mol. Simul.*, 2006, **32**(14), 1187–1193.

58 C. Wang, V. Kondrashchenko and A. Matseevich, Prediction of the coefficient of thermal expansion of building materials based on polyvinyl chloride,, *J. Phys.: Conf. Ser.*, 2019, 012094.

59 H. Jayanna and S. Subramanyam, Thermal expansion of irradiated polyvinyl chloride from 10 K to 340 K, *Polym. Bull.*, 1992, **28**(4), 481–487.

60 C. B. Potter, M. T. Davis, A. B. Albadarin and G. M. Walker, Investigation of the dependence of the Flory–Huggins interaction parameter on temperature and composition in a drug–polymer system, *Mol. Pharm.*, 2018, **15**(11), 5327–5335.

61 A. J. Nedoma, M. L. Robertson, N. S. Wanakule and N. P. Balsara, Measurements of the composition and molecular weight dependence of the Flory−Huggins interaction parameter, *Macromolecules*, 2008, **41**(15), 5773–5779.

62 J. M. Tesha, Molecular Dynamics Simulation of Polysulfone and Polystyrene-co-maleic Anhydride Blends Compatibility: A mesoscopic, Ewald Approach and Experimental Comparison, *Research Square*, 2021, preprint, DOI: 10.21203/rs.3.rs-1109742/v1.